

Lipid Membrane Deformation Accompanied by Disk-to-Ring Shape Transition of Cholesterol-Rich Domains

Yong-Sang Ryu,[†] Daehan Yoo,^{†,∇} Nathan J. Wittenberg,^{†,∇} Luke R. Jordan,[‡] Sin-Doo Lee,[§] Atul N. Parikh,^{||} and Sang-Hyun Oh^{*,†,‡}

[†]Departments of Electrical and Computer Engineering and [‡]Biomedical Engineering, University of Minnesota, Minneapolis, Minnesota 55455, United States

[§]School of Electrical Engineering, Seoul National University, Seoul, Republic of Korea 151-742

^{||}Departments of Biomedical Engineering and Chemical Engineering & Materials Science, University of California, Davis, California 95616, United States

S Supporting Information

ABSTRACT: During vesicle budding or endocytosis, biomembranes undergo a series of lipid- and protein-mediated deformations involving cholesterol-enriched lipid rafts. If lipid rafts of high bending rigidities become confined to the incipient curved membrane topology such as a bud-neck interface, they can be expected to reform as ring-shaped rafts. Here, we report on the observation of a disk-to-ring shape morpho-chemical transition of a model membrane in the absence of geometric constraints. The raft shape transition is triggered by lateral compositional heterogeneity and is accompanied by membrane deformation in the vertical direction, which is detected by height-sensitive fluorescence interference contrast microscopy. Our results suggest that a flat membrane can become curved simply by dynamic changes in local chemical composition and shape transformation of cholesterol-rich domains.

Lipid bilayer membranes are two-dimensional fluids consisting of dynamic assemblies of lipids and proteins and serve as the boundaries of cells and organelles. Many crucial cellular processes involve structural changes in membrane shape via coupling of the membrane curvature with the chemical composition. Some examples include endo- or exocytosis, release of enveloped viruses, synaptic activity regulation, and vesicle budding from intracellular organelles.¹ In general, such cellular processes are not spontaneous, often requiring the assistance of specialized proteins (Clathrin and COP-I and II proteins).² Dissecting the roles that membrane physicochemical properties play in facilitating these protein-mediated membrane deformations is difficult in living cells. To this end, model membrane systems, for example, supported lipid bilayers (SLBs) and giant vesicles, allow precise tailoring of the membrane composition as well as its curvature independently. Lipid rafts are dynamic domains in cell membranes that are enriched in cholesterol (CHOL), sphingolipids (SM), and saturated phospholipids.^{1b} They serve as membrane organizing centers and are thought to be associated with cell signaling, vesicle budding, and virus entry among other processes.³ In model membranes, CHOL and SM-rich liquid-ordered (l_o) domains mimic cellular rafts on a

micrometer scale recapitulating their essential physical properties (i.e., thickness, rigidity, curvature, and compressibility, etc.)⁴ relative to the background liquid-disordered (l_d) phase, which is primarily composed of unsaturated phospholipids. A number of groups have experimentally⁵ and theoretically³ investigated the relationship between the l_o domains and membrane curvature: Some found that the l_o domains favor relatively low curvature membrane zones,⁶ whereas others demonstrated that the l_o domains are isolated in regions with locally negative curvatures^{5c,d} imparted by CHOL. It has been theoretically predicted that the line tension and lateral pressure of the l_o domains and their interplay with the curvature elastic energies can drive membrane budding.⁷ Provided that the l_o domains surround a bud-neck region and maintain their interleaflet compositional asymmetry,^{7b} they can adopt a ring-type morphology^{4b} as reported previously using a bud-mimicking template.^{5c} However, spontaneous compositional remodeling of l_o domains and subsequent structural transformation into ring-shapes during membrane deformation have not been observed in model membrane systems. Living cell membranes are dynamic structures that actively remodel their shapes. Thus, it is important to explore spontaneous formation of ring-raft domains driven by membrane's internal compositional degrees of freedom unaided by templating effects of the underlying substrates. Such substrate-independent morphological remodeling is analogous to the behavior of cellular membranes in the early stage of endocytosis^{5c} without the aid of the coat proteins.^{1b,2}

In this work, we observed that above a critical dimension, a l_o domain in a planar SLB undergoes a morpho-chemical transition from a disk-to-ring shape. This is accompanied by membrane deformation away from the underlying substrate in the form of a spherical cap-like structure (Figure 1a). To characterize the three-dimensional (3D) membrane deformation after shape transition via height-sensitive fluorescence interference contrast (FLIC) microscopy, we engineered a SiO₂-coated gold substrate consisting of a smooth circular region (S) and a surrounding rough region (R) (Figure 1b,c). The patterned surface was prepared by combining photolithography, template stripping,⁸ and atomic layer deposition (ALD). A 150 nm-thick gold film

Received: May 1, 2015

Published: June 8, 2015

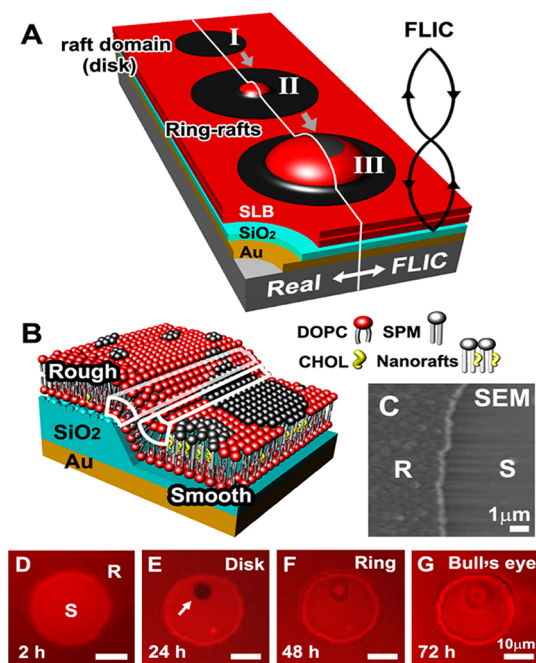


Figure 1. Spontaneous disk-to-ring shape transition of an l_o domain observed using FLIC microscopy. (a) Illustration of an l_o domain undergoing a disk (I)-to-ring (II) transition, accompanied by deformation of the SLB (III). The actual morphology and the corresponding FLIC image are shown. (b) Illustration of the rough (R) and smooth (S) regions covered with a SLB showing the coalescence of l_o domains in the smooth regions. (c) Scanning electron micrograph of R and S regions. (d) Fluorescence image of a SLB with R and S regions after 2 h. Fluorescence contrast arises from the differential thickness of the SiO_2 layer, leading to FLIC. (e) The l_o domain (indicated by the arrow) was formed after 24 h. (f) After 48 h, the disk shape of the l_o domain spontaneously transformed into a ring-shape. (g) After 72 h, a bull's eye interference pattern was observed, indicating that the membrane inside the ring was raised up from the substrate.

under the 50 nm-thick layer of SiO_2 acts as a mirror to satisfy the conditions for the FLIC (Supporting Information Figure S1). After fabrication, a PDMS fluidic chip was attached to the substrates to keep membranes fully hydrated for the duration of experiments (Figure S2). On the patterned surface, the l_o phase coarsens atop the smooth circular region according to the elastic energy sorting mechanism confirmed previously.^{5d} In contrast to the uniform growth of the l_o domain over the entire area of the smooth region, as observed in the previous work,^{5d} in the present work the coalescence of small circular l_o domains was clearly observed. Figure 1d shows a fluorescence image of a SLBs composed of dioleoylphosphatidylcholine (DOPC), SM, CHOL, and Texas Red-labeled phosphatidylethanolamine (TR-DHPE), in a 40/40/19/1 molar ratio 2 h after its formation by vesicle rupture. The differential brightness is due to the thicker SiO_2 in the rough region, which leads to the destructive interference of the fluorescence emission via FLIC. Fluorescence recovery after photobleaching (FRAP) measurements confirmed the lateral fluidity and continuity ($D = 0.89 \pm 0.2 \mu\text{m}^2/\text{s}$; Figure S3) of the SLB. At the lipid composition we used, the SLB is known to phase separate at room temperature.^{5c,d} Since the TR-DHPE molecules prefer the l_d phase, dark spots seen in the SLB correspond to the l_o phase domains. This is evident by the lack of dark spots in a SLB on an identical substrate composed of a lipid mixture which does not form domains (Figure S4). A disk-shaped l_o domain was observed 24 h after formation (Figure 1e).

After 48 h, the l_o domain transitions into a ring shape (Figure 1f), and after 72 h, a bull's eye feature appeared (Figure 1g). One or two disk-shaped l_o domains per smooth zone were formed near the smooth-rough boundaries after 12 h (Figure 2a). Previous

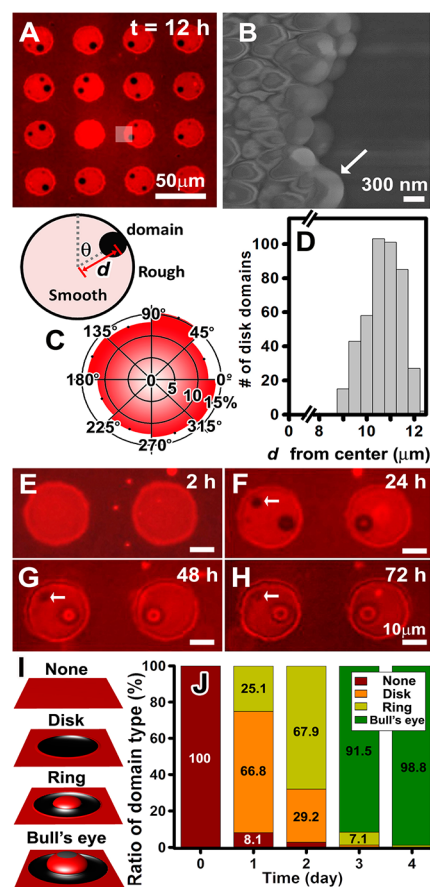


Figure 2. Nucleation, growth, and shape change of l_o domains. (a) Fluorescence image showing a 12 h-old SLB over 16 separate smooth areas wherein disk-shaped l_o domains formed. There were two or fewer l_o domains in every area examined. (b) SEM image of the boundary between smooth (right) and rough (left) surfaces. Nanoscale defects, indicated by an arrow, can serve as nucleation sites for l_o domain ripening. (c) Angular histogram shows that l_o domains were distributed at random angles in the smooth areas. (d) Histogram showing the distribution of d , the distance from the center of the smooth areas to the center of l_o domains. There is a clear tendency for formation near the edges. Formation of disk-shaped l_o domains (e), their transition to ring-shaped domains (f), and subsequent formation of bull's eye structures (g, h). (i) Conceptual illustration: the appearance of bud-shaped membrane structures in FLIC microscopy. (j) Proportion of l_o domains that appear as a disk, ring, or bull's eye as a function of time.

work^{5d} with similar substrates showed that the l_o domains typically grew from the edges inward and no circular domains were observed. Instead, the l_o domains gradually ripened homogeneously to completely fill the smooth area. Here, local defects in the boundaries between smooth and rough zones, such as the inflexed arch shown in Figure 2b, may serve as seed sites for the coalescence of the disk-shape l_o domains accounting for the distinct behavior of the l_o domain as compared to the previous work.^{5d} The l_o domains were formed randomly around the smooth zone perimeter as shown by the angular histogram in Figure 2c and generally developed near the perimeter, as seen in the histogram in Figure 2d. A plausible reason that the l_o domains

tend to form at the edges is because of the large negative spontaneous curvature of the l_o domain ($c_o = -1/68 \text{ \AA}^{-1}$) compared to the l_d phase ($c_d = -1/160 \text{ \AA}^{-1}$).^{5c} The boundary between the smooth and rough substrate causes an elastic distortion of the membrane, which is relaxed by gathering the l_o domains with large negative spontaneous curvature at sites of negative substrate curvature (Figures 1b and S5). We observed that the l_o phase domains grew in a disk-like fashion, reducing the total line tension arising from the thickness mismatch between the l_o and l_d phases⁹ by reducing the length of the l_o - l_d interface.

We found that upon reaching a critical size (average radius of $\sim 3.9 \mu\text{m}$; Figure S7), a disk-shaped l_o domain becomes unstable, transforming first into a characteristic ring shape (donut shape) and ultimately into a bull's eye pattern as witnessed in the fluorescence images (Figure 2e–h). The fluorescence image after 24 h shows a dark ring (the l_o domain) encircling a bright spot, which suggests that in the l_d phase, lipids and TR-DHPE migrate into the center of the structure. After at least 48 h, the structure began to appear as a bull's eye, which suggests the bright patch of the l_d membrane encircled by the l_o ring is deformed to move further away from the underlying gold mirror. This results in a dimming center due to the FLIC effect. In addition, in cases with multiple disk l_o phase domains in a smooth region, the smaller domains disappear as larger ones grow akin to Ostwald ripening (see the arrows in Figure 2e–h). The relative proportion of a disk-, ring-, or bull's eye-shaped l_o domain (Figure 2i) as a function of time is shown in Figure 2j.

Next, we fit the fluorescence intensity profile of the bull's eye-type structures to an established FLIC model to determine the z -axis displacement of the membrane.¹⁰ In our images, the dark features arise from two sources, one of which is concentration based and the other is interference based. The concentration-based source of darkness is exclusion of TR-DHPE fluorophore from the l_o domain. The interference-based darkness arises from the height-dependent destructive interference of fluorescence emission due to the z -axis height of the deformed patch of the SLB inside the ring-type l_o domain. Figure 3a shows the evolution of the l_o domain from a disk, a ring to a bull's eye over 12 to 72 h. After 96 h, the structure shows two FLIC bands: a ring and a point in the center (Figure 3b). We plotted the intensity profile of the fringe pattern ($t = 96 \text{ h}$) along the line in Figure 3c. Assuming that the l_o domain ring, which forms the boundary of the deformed membrane, has an inner radius of $\sim 5.5 \mu\text{m}$, and the deformed membrane is shaped like a spherical cap, we fit the fluorescence intensity profile (F) to the following equation to determine h , the height of the membrane above the substrate, as a function of the radius:^{10d}

$$F = \sin^2\left(\frac{2\pi(n_w h + n_o h_o)}{\lambda_{\text{ex}}}\right) \sin^2\left(\frac{2\pi(n_w h + n_o h_o)}{\lambda_{\text{em}}}\right) \quad (1)$$

where h_o is the oxide thickness, n_w and n_o are the refractive indices of water (1.33) and silica (1.46), respectively. The λ_{ex} and λ_{em} indicate the excitation (560 nm) and emission (645 nm) wavelengths, respectively. The shape profile of membrane deformation inside the ring-type l_o domain obtained from eq 1 is plotted in Figure 3d. The fit shows that the deformed membrane has a maximum height of $\sim 338 \text{ nm}$ above the substrate. We assumed a spherical-cap geometry because it has uniform curvature over its surface and thus is the minimum energy conformation for a curved membrane given the constraints of our system.

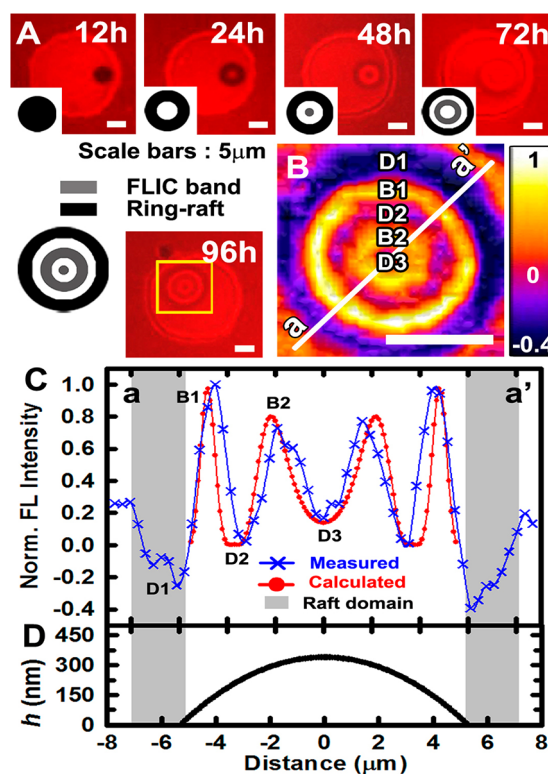


Figure 3. Membrane deformation after l_o domain disk-to-ring transition and 3D topography determined by FLIC microscopy. (a) The evolution of l_o domains from disk to ring shape with illustrations (inset) over the course of 96 h. The outermost black features represent darkness arising from exclusion of TR-DHPE fluorophore from the ring-type l_o domains. The gray features represent apparent darkness arising from destructive interference in the FLIC image. (b) Normalized fluorescence intensity profile of the boxed area ($t = 96 \text{ h}$) shows alternating patterns with dark (D) and bright (B) zones. (c) Fluorescence intensity profile (blue curve) across a l_o domain ring matches well with the calculated fluorescent intensity profile (red curve) obtained from eq 1 except the outer rings (D1 zone). The darkest features of the FLIC microscopy images, the outer rings, do not agree well with the intensity profile predicted by FLIC theory, strengthening our argument that these rings arise due to exclusion of TR-DHPE from the l_o domain, rather than destructive interference. Furthermore, the l_o domains and bull's eye features disappear when the sample is heated above the phase transition temperature of the membrane, suggesting that the observed deformation is mediated by the presence of l_o domains (Figure S8). (d) Actual SLB geometry of the deformed SLB was obtained by calculating the fluorescence profile using eq 1. The fluorescence intensity profiles and calculated SLB geometry at intermediate time points (24, 48, 72 h) are shown in Figure S9.

This size-dependent, disk-to-ring shape transition of the membrane domains accompanied by the appearance of localized bud topography requires considerations of both the energetics and dynamics specific to the raft formation under the control of substrate topography. Energetically, the l_o phase domain embedded in the l_d phase surroundings introduces line tension energy. This line tension arises because the l_o phase is $\sim 1 \text{ nm}$ thicker than the l_d phase,⁹ resulting in partial exposure of the lipid backbone of the l_o phase to water. Microscopically, energetically unfavorable partial lipid backbone exposure due to thickness difference at the l_o/l_d boundary gives rise to local splay and tilt elastic deformations in the vicinity of the domain boundaries.^{7d} The line tension energy, which is estimated for raft domains in fluid lipid surroundings to be a $\sim 1 \text{ pN}$ for a monolayer height

mismatch of 0.3 nm,^{5a} increases in proportion to the length of the domain boundary. In contrast, the curvature bending energy is independent of the domain size. Moreover, such out-of-plane deformation of single domains reduces the boundary length and thus lowers the line tension contribution to the total membrane energy.^{7a} Thus, above a critical domain size, bud formation becomes energetically favorable. Interestingly, however, our observations reveal that the length of the boundary between the co-existing phases is increased suggesting the role of microscopic reorganization of membrane domains. The observed disk-to-ring transformation indicates that the l_o domains are accumulated at the bud-neck region and gradually expelled from the positive curvature topography of the bud surface. We surmise that this dynamic domain reorganization is prompted by the pattern of curvatures generated by the bud-like geometry. This is not surprising since raft domains have negative spontaneous curvature and are known to concentrate, especially, with composition asymmetry in the bud-neck region.^{5c}

Alternatively, during the domain growth process, compositional heterogeneity inside the l_o domain may drive the disk-to-ring shape transition. The building blocks of the l_o domain, i.e., cholesterol-sphingomyelin units, arrive by diffusion and join the l_o domain at the perimeter. Due to significantly reduced diffusion coefficients of lipids inside the l_o domain,¹¹ diffusion within the l_o domains is slower than the rate at which l_o domain building blocks coalesce with existing l_o domains. This generates a concentration gradient of CHOL and SM from lower near the center to higher along the perimeter of a l_o domain. When the gradient reaches critical limits, the l_o domain may remodel and transform its shape. This is because elimination of the gradient to form a ring domain by creating another l_d/l_o boundary around the inner rim of the ring may be more energetically favorable than the line tension penalty from larger disk-shaped l_o domains. Additional work is needed to address this possibility.

In conclusion, we observed the spontaneous remodeling of l_o domains from disk-to ring shape accompanied by membrane deformations that are analogous to deformations in cells. Our discovery of 3D ring-rafts formation that are not driven by the topography of the underlying substrate^{5c} but by self-assembly of particular lipid components sheds light upon raft domain involvement in processes associated with changes in membrane shape, like endocytosis.^{1b,2} Our combination of silica-coated metal substrates with smooth/rough topographies and height-sensitive FLIC imaging offers new methods to unravel the complex biophysical dynamics of curvature-composition coupling associated with raft domains. This platform could also be integrated with label-free surface-based detection methods such as surface plasmon resonance and surface-enhanced spectroscopies.¹²

■ ASSOCIATED CONTENT

Supporting Information

Details on sample fabrication, lipid membrane preparation, FLIC microscopy, and deformation energy calculation. The Supporting Information is available free of charge on the ACS Publications website at DOI: 10.1021/jacs.5b04559.

■ AUTHOR INFORMATION

Corresponding Author

*sang@umn.edu

Author Contributions

^V(D.Y., N.J.W.) These authors contributed equally.

Notes

The authors declare no competing financial interest.

■ ACKNOWLEDGMENTS

This work was supported by grants from the National Institutes of Health (R01 GM092993; N.J.W., L.R.J., S.H.O.), National Science Foundation (CAREER Award; Y.S.R., D.Y., S.H.O.), MnDrive Research Initiative (N.J.W. and S.H.O.), Department of Energy (BES #DEFG02-04ER46173; A.N.P.), and the Brain Korea 21 Plus Project 2014 (S.D.L.).

■ REFERENCES

- (1) (a) Zhang, J.; Xue, R.; Ong, W.-Y.; Chen, P. *Biophys. J.* **2009**, 97, 1371. (b) Chazal, N.; Gerlier, D. *Microbiol. Mol. Biol. Rev.* **2003**, 67, 226. (c) Rosa, P.; Fratangeli, A. *Commun. Integr. Biol.* **2010**, 3, 352. (d) Rothman, J. E.; Orci, L. *Sci. Am.* **1996**, 274, 70.
- (2) (a) Pinot, M.; Goud, B.; Manneville, J.-B. *Mol. Membr. Biol.* **2010**, 27, 428. (b) Votteler, J.; Sundquist, W. I. *Cell Host Microbe* **2013**, 14, 232.
- (3) Reynwar, B. J.; Illya, G.; Harmandaris, V. A.; Müller, M. M.; Kremer, K.; Deserno, M. *Nature* **2007**, 447, 461.
- (4) (a) Harder, T.; Simons, K. *Curr. Opin. Cell Biol.* **1997**, 9, 534. (b) Huttner, W. B.; Zimmerberg, J. *Curr. Opin. Cell Biol.* **2001**, 13, 478.
- (5) (a) Baumgart, T.; Hess, S. T.; Webb, W. W. *Nature* **2003**, 425, 821. (b) Kaizuka, Y.; Groves, J. T. *New J. Phys.* **2010**, 12, 11. (c) Ryu, Y.-S.; Lee, I.-H.; Suh, J.-H.; Park, S.; Oh, S.; Jordan, L. R.; Wittenberg, N. J.; Oh, S.-H.; Jeon, N.; Lee, B.; Parikh, A. N.; Lee, S.-D. *Nat. Commun.* **2014**, 5, 4507. (d) Yoon, T.-Y.; Jeong, C.; Lee, S.-W.; Kim, J.; Choi, M. C.; Kim, S.-J.; Kim, M. W.; Lee, S.-D. *Nat. Mater.* **2006**, 5, 281.
- (6) (a) Subramaniam, A.; Lecuyer, S.; Ramamurthi, K. S.; Losick, R.; Stone, H. A. *Adv. Mater.* **2010**, 22, 2142. (b) Parthasarathy, R.; Yu, C.-H.; Groves, J. T. *Langmuir* **2006**, 22, 5095.
- (7) (a) Lipowsky, R. *Biophys. J.* **1993**, 64, 1133. (b) Larsen, J. B.; Jensen, M. B.; Bhatia, V.; Pedersen, S. L.; Bjørnholm, T.; Iversen, L.; Uline, M.; Szleifer, I.; Jensen, K. J.; Hatzakis, N. S.; Stamou, D. *Nat. Chem. Biol.* **2015**, 11, 192. (c) Andes-Koback, M.; Keating, C. D. *J. Am. Chem. Soc.* **2011**, 133, 9545. (d) Kuzmin, P. I.; Akimov, S. A.; Chizmadzhev, Y. A.; Zimmerberg, J.; Cohen, F. S. *Biophys. J.* **2005**, 88, 1120. (e) García-Sáez, A. J.; Chiantia, S.; Schwill, P. *J. Biol. Chem.* **2007**, 282, 33537.
- (8) Nagpal, P.; Lindquist, N. C.; Oh, S.-H.; Norris, D. J. *Science* **2009**, 325, 594.
- (9) (a) Sprong, H.; van der Sluijs, P.; van Meer, G. *Nat. Rev. Mol. Cell Biol.* **2001**, 2, 504. (b) Heberle, F. A.; Petruziello, R. S.; Pan, J.; Drazba, P.; Kučerka, N.; Standaert, R. F.; Feigenson, G. W.; Katsaras, J. *J. Am. Chem. Soc.* **2013**, 135, 6853.
- (10) (a) Ajo-Franklin, C. M.; Yoshina-Ishii, C.; Boxer, S. G. *Langmuir* **2005**, 21, 4976. (b) Crane, J. M.; Kiessling, V.; Tamm, L. K. *Langmuir* **2005**, 21, 1377. (c) Hoopes, M. I.; Faller, R.; Longo, M. L. *Langmuir* **2011**, 27, 2783. (d) Wong, A. P.; Groves, J. T. *J. Am. Chem. Soc.* **2001**, 123, 12414.
- (11) Kahya, N.; Scherfeld, D.; Bacia, K.; Poolman, B.; Schwill, P. *J. Biol. Chem.* **2003**, 278, 28109.
- (12) (a) Im, H.; Wittenberg, N. J.; Lesuffleur, A.; Lindquist, N. C.; Oh, S.-H. *Chem. Sci.* **2010**, 1, 688. (b) Brolo, A. G.; Kwok, S. C.; Moffitt, M. G.; Gordon, R.; Riordon, J.; Kavanagh, K. L. *J. Am. Chem. Soc.* **2005**, 127, 14936. (c) Dahlin, A.; Zäch, M.; Rindzevicius, T.; Käll, M.; Sutherland, D. S.; Höök, F. *J. Am. Chem. Soc.* **2005**, 127, 5043. (d) Reimhult, E.; Larsson, C.; Kasemo, B.; Höök, F. *Anal. Chem.* **2004**, 76, 7211.